The relationship between two fast/slow analysis techniques for bursting oscillations

Wondimu Teka, Joël Tabak, and Richard Bertram

Related Articles

Amplitude equation for a diffusion-reaction system: The reversible Sel'kov model
AIP Advances 2, 042125 (2012)

Nonlinear multimode dynamics and internal resonances of the scan process in noncontacting atomic force microscopy
J. Appl. Phys. 112, 074314 (2012)

Secondary nontwist phenomena in area-preserving maps
Chaos 22, 033142 (2012)

Bifurcation theory for the L-H transition in magnetically confined fusion plasmas
Phys. Plasmas 19, 072309 (2012)

Billiards with a given number of (k,n)-orbits
Chaos 22, 026109 (2012)

Additional information on Chaos

The relationship between two fast/slow analysis techniques for bursting oscillations

Wondimu Teka,[1] Joël Tabak,[2] and Richard Bertram[3,a]
[1]*Department of Mathematics, Florida State University, Tallahassee, Florida 32306, USA*
[2]*Department of Biological Science, Florida State University, Tallahassee, Florida 32306, USA*
[3]*Department of Mathematics, and Programs in Neuroscience and Molecular Biophysics, Florida State University, Tallahassee, Florida 32306, USA*

Bursting oscillations in excitable systems reflect multi-timescale dynamics. These oscillations have often been studied in mathematical models by splitting the equations into fast and slow subsystems. Typically, one treats the slow variables as parameters of the fast subsystem and studies the bifurcation structure of this subsystem. This has key features such as a z-curve (stationary branch) and a Hopf bifurcation that gives rise to a branch of periodic spiking solutions. In models of bursting in pituitary cells, we have recently used a different approach that focuses on the dynamics of the slow subsystem. Characteristic features of this approach are folded node singularities and a critical manifold. In this article, we investigate the relationships between the key structures of the two analysis techniques. We find that the z-curve and Hopf bifurcation of the two-fast/one-slow decomposition are closely related to the voltage nullcline and folded node singularity of the one-fast/two-slow decomposition, respectively. They become identical in the double singular limit in which voltage is infinitely fast and calcium is infinitely slow. © *2012 American Institute of Physics*. [http://dx.doi.org/10.1063/1.4766943]

Bursting electrical oscillations are common in nerve cells and endocrine cells. These consist of episodes of electrical activity followed by periods of quiescence. Since each electrical impulse is itself an oscillation, this is an example of a multi-time scale oscillation, which has been analyzed successfully using a decomposition of the system of equations into fast and slow subsystems. In this article, we compare two alternate fast/slow analysis techniques for the study of the type of bursting oscillations that typically occur in pituitary lactotrophs and somatotrophs. We show the relationships between the key elements of both types of analysis.

I. INTRODUCTION

Bursting oscillations are common patterns of electrical activity in excitable cells such as neurons[1–5] and many endocrine cells.[6–10] Bursting activity is characterized by alternation between periods of spiking and periods of rest, and is driven by slow variations in one or more slowly changing variables, such as the intracellular calcium concentration. Bursting oscillations are often more efficient than tonic spiking in mediating the release of neurotransmitter or hormone.[7,8,11] Many mathematical models have been developed to study various aspects of the dynamics of bursting oscillations.[2,9,12–16] In many cases, the bursting dynamics have been analyzed by dividing the system into fast and slow subsystems such that the slow subsystem includes a single slow variable, and the fast subsystem includes the remaining variables, which are relatively fast. When the system is three-dimensional, we refer to this technique as a "two-fast/one-slow analysis." Recently, we used a different approach for the analysis of bursting that formally divides the three variables into a one-dimensional fast subsystem and a two-dimensional slow subsystem.[17,18] The main goal of this paper is to clarify the relationship between the now-standard two-fast/one-slow analysis and the new one-fast/two-slow analysis.

In the standard two-fast/one-slow analysis, one studies the dynamics of the fast subsystem with the slow variable treated as a parameter.[19–24] The bifurcation structure of the fast subsystem with the slow variable as the bifurcation parameter consists of the z-curve (set of fast subsystem stationary solutions); fast subsystem periodic solutions; and Hopf, saddle-node, and homoclinic bifurcations (HM). Bursting oscillations are then understood by superimposing the burst trajectory onto the fast subsystem bifurcation diagram. This approach has been very successful for understanding bursting in pancreatic islets[25] and neurons.[2–4,21] It has also been useful in understanding various aspects of bursting in pituitary cells such as resetting properties,[26] how fast subsystem manifolds affect burst termination,[23] and how parameter changes convert the system from one burst type to the other.[24]

In the alternate one-fast/two-slow analysis, one associates a variable with an intermediate time scale with the slow subsystem rather than the fast subsystem. Analysis is then performed on the planar slow subsystem, rather than the planar fast subsystem of the standard decomposition. This approach is typically used to study canard induced

mixed-mode oscillations.[27–29] These oscillations are due to the existence of a folded node (FN) singularity of the slow subsystem.[17,18,27,28,30,31]

Using a model of the electrical activity of pituitary lactotrophs,[18] we provide a comparative analysis of the two techniques (two-fast/one-slow and one-fast/two-slow). In particular, we show the relationship between the z-curve and the voltage nullcline of the planar slow subsystem. We also show the relationship between the Hopf bifurcation (HB) that gives rise to a branch of spiking solutions in the two-fast/one-slow analysis and the folded node singularity that is responsible for the spiking oscillations in the one-fast/two-slow analysis.

II. THE MATHEMATICAL MODEL

We use a model of the pituitary lactotroph, which produces what has been called "pseudo-plateau bursting" (PPB) over a range of parameter values.[18] This bursting has small spikes emanating from a depolarized voltage plateau, as is typically observed in pituitary lactotrophs and somatotrophs.[6–9] The details of the model and the parameter values are given in the Appendix. The model includes three variables: V (membrane potential), n (fraction of activated delayed rectifier K$^+$ channels), and c (cytosolic free Ca^{2+} concentration). The equations are

$$C_m \frac{dV}{dt} = -(I_{Ca} + I_K + I_{K(Ca)} + I_{BK}), \quad (1)$$

$$\frac{dn}{dt} = \frac{n_\infty(V) - n}{\tau_n}, \quad (2)$$

$$\frac{dc}{dt} = -f_c(\alpha I_{Ca} + k_c c), \quad (3)$$

where I_{Ca} is an inward Ca^{2+} current, I_K is an outward delayed rectifying K$^+$ current, $I_{K(Ca)}$ is a small-conductance Ca^{2+}-activated K$^+$ current, and I_{BK} is a fast-activating large-conductance BK-type K$^+$ current. Expressions for the ionic currents are

$$I_{Ca} = g_{Ca} m_\infty(V)(V - V_{Ca}), \quad (4)$$

$$I_K = g_K n(V - V_K), \quad (5)$$

$$I_{K(Ca)} = g_{K(Ca)} s_\infty(c)(V - V_K), \quad (6)$$

$$I_{BK} = g_{BK} b_\infty(V)(V - V_K). \quad (7)$$

All numerical simulations and bifurcation diagrams (both one- and two-parameter) were constructed using the XPPAUT software package,[32] using the Runge-Kutta integration method, and computer codes can be downloaded as freeware from http://www.math.fsu.edu/~bertram/software/pituitary.

III. TWO-FAST/ONE-SLOW ANALYSIS

Figure 1(a) shows the pseudo-plateau bursting pattern produced by the model. The bursting pattern is accompanied by the slow variation of c that increases during the active phase and decreases during the silent phase of the burst.

The three variables (Eqs. (1)–(3)) vary on different time scales, and variables V and n are much faster than c (for details, see the Appendix). By taking advantage of time scale separation, the system can be divided into fast and slow subsystems, and the dynamics can be analyzed using a two-fast/one-slow analysis. Here, c is treated as a parameter of the fast subsystem, which consists of the fast variables V and n. A bifurcation diagram summarizing the equilibrium dynamics of the fast subsystem is then constructed using c as
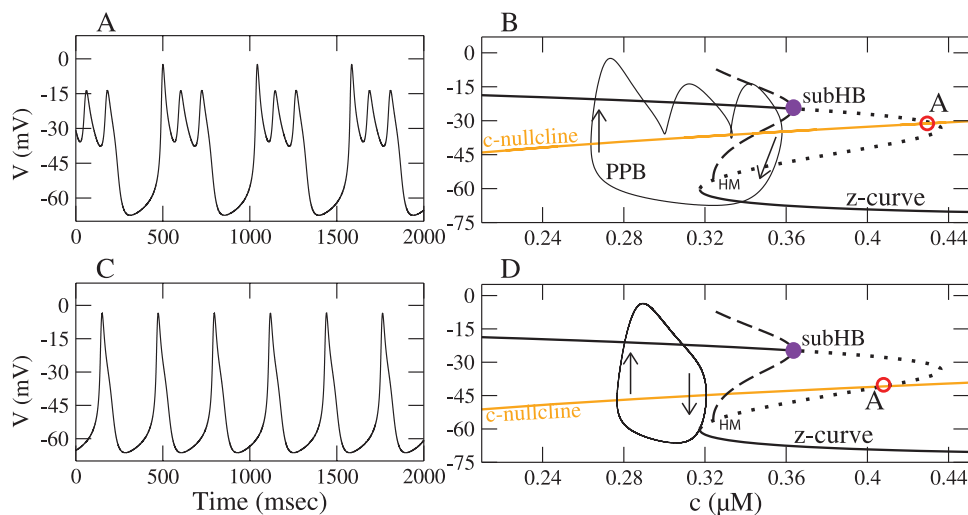

FIG. 1. Two-fast/one-slow analyses for pseudo-plateau bursting and spiking patterns with parameter values $g_K = 4$ nS, $g_{BK} = 0.4$ nS, and $C_m = 10$ pF. (a) Pseudo-plateau bursting produced with $k_c = 0.16 \, (\text{ms})^{-1}$. (b) The fast subsystem bifurcation structure for pseudo-plateau bursting. The superimposed pseudo-plateau burst trajectory (PPB curve) and c-nullcline are produced with $k_c = 0.16 \, (\text{ms})^{-1}$. (c) Continuous spiking with $k_c = 0.1 \, (\text{ms})^{-1}$. (d) The bifurcation structure for a continuous spiking pattern and a superimposed spiking trajectory with $k_c = 0.1 \, (\text{ms})^{-1}$. When k_c is decreased, the c-nullcline moves downward, causing a transition from bursting to spiking. In panel (b) and (d), an unstable limit cycle (dashed curve) emerges from a subcritical HB, and terminates at a HM. The full three-dimensional system has an unstable equilibrium point ((a), unfilled circle). For panel (a) and (c), and for the superimposed trajectories, $f_c = 0.01$.

the bifurcation parameter.[19,21–24] Figure 1(b) shows the fast subsystem bifurcation structure for pseudo-plateau bursting. The "z-curve" that represents the stationary solutions of the fast subsystem has three branches that are connected by saddle-node bifurcations, or knees. The upper branch that has unstable (dotted) and stable (solid) portions corresponds to the depolarized (high-voltage) steady states, and the lower branch that consists of stable nodes represents the hyperpolarized (low-voltage) steady states. The middle branch consists of saddle points. The system is bistable between the stable lower and upper steady states for a range of c values. A branch of unstable periodic solutions (dashed curve) emerges from a subcritical Hopf bifurcation (subHB) and terminates at a HM.

The dynamics of pseudo-plateau bursting can be analyzed using the (c, V)-plane as a phase plane, and by treating the z-curve as a generalized V-nullcline. The z-curve and the c-nullcline (orange curve), where $dc/dt = 0$, are projected into the (c, V)-phase plane, and they intersect at an unstable equilibrium point of the full system (point A, unfilled circle). The trajectory of the full (three-dimensional) system (the pseudo-plateau bursting orbit) is then superimposed (PPB curve, Fig. 1(b)). Note that $dc/dt < 0$ and $dc/dt > 0$ below and above the c-nullcline, respectively. As a result, the flow of the trajectory when V is low is leftward, and the flow when V is high is rightward. If c were a truly slow variable the trajectory would form a hysteresis cycle over the bistable interval, producing a relaxation oscillation. However, c is only marginally slow, so the silent phase of the burst trajectory hardly follows the lower branch of the z-curve, and it overshoots the lower knee. The trajectory then exhibits small oscillations about the stable upper branch of weakly stable foci.

The bursting can be converted to continuous spiking by reducing the Ca^{2+} pump rate k_c, thus, lowering the c-nullcline (Figs. 1(c) and 1(d)). It is neither apparent from the two-fast/one-slow analysis why this transition occurs, nor is it clear why the spiking orbit no longer follows the z-curve at all. What is apparent is that the two-fast/one-slow analysis has limited predictive power for this system.

IV. ONE-FAST/TWO-SLOW ANALYSIS

Rather than associating n with the fast subsystem, as above, one could associate it with c in the slow subsystem. The time-scale separation between V and the slow variables n and c can be accentuated by reducing the membrane capacitance C_m, which makes V even faster. In the singular limit $C_m \to 0$, the trajectories follow a two-dimensional surface called the critical manifold and given by

$$S \equiv \{(V, c, n) \in \mathbb{R}^3 : f(V, c, n) = 0\}, \quad (8)$$

where

$$f(V, c, n) = -(I_{Ca} + I_K + I_{K(Ca)} + I_{BK}). \quad (9)$$

The critical manifold has three sheets that are separated by fold curves (L^- and L^+) (Fig. 2). The lower and upper sheets are attracting $\left(\frac{\partial f}{\partial V} < 0\right)$ and the middle sheet is
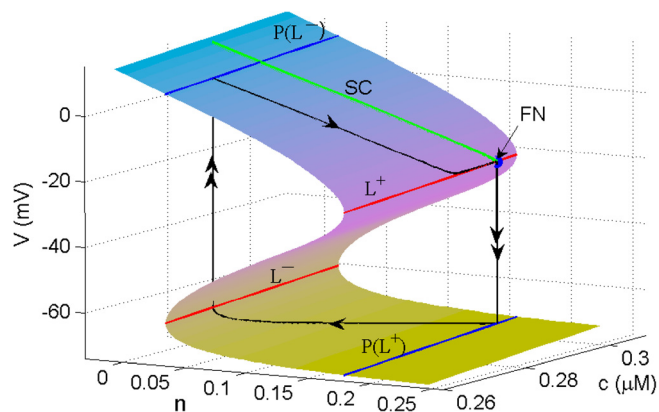

FIG. 2. The critical manifold and fold curves with their projections for $g_K = 4\,\text{nS}$, $g_{BK} = 0.4\,\text{nS}$, $f_c = 0.01$, and $k_c = 0.16\,(\text{ms})^{-1}$. L^- and L^+ are the lower and upper fold curves. $P(L^-)$ and $P(L^+)$ are the projections of L^- and L^+ onto the upper and lower sheets of the critical manifold, respectively. The curve SC (green curve) is the strong canard, and FN is a folded node singularity. The singular periodic orbit (black curve with arrows) is superimposed on the critical manifold.

repelling $\left(\frac{\partial f}{\partial V} > 0\right)$. The lower ($L^-$) and upper ($L^+$) fold curves are given by

$$L^\pm \equiv \left\{ (V, c, n) \in \mathbb{R}^3 : f(V, c, n) = 0 \right.$$
$$\left. \text{and} \quad \frac{\partial f}{\partial V}(V, c, n) = 0 \right\}. \quad (10)$$

By differentiating $f(V, c, n) = 0$ with respect to time and then introducing a rescaled time $\tau = -\left(\frac{\partial f}{\partial V}\right)^{-1} t$, one obtains a desingularized system that describe the flow on the surface S

$$\frac{dV}{d\tau} = F(V, c, n), \quad (11)$$

$$\frac{dc}{d\tau} = f_c(\alpha I_{Ca} + k_c c)\frac{\partial f}{\partial V}, \quad (12)$$

where

$$F(V, c, n) = (-f_c(\alpha I_{Ca} + k_c c))\frac{\partial f}{\partial c} + \left(\frac{n_\infty(V) - n}{\tau_n}\right)\frac{\partial f}{\partial n}, \quad (13)$$

where n satisfies $f(V, c, n) = 0$. The derivation of the desingularized system is given in Ref. 18. These equations describe the flow on the upper and lower attracting sheets in the limit $C_m \to 0$.

The equilibria of the desingularized system can be of two types. First, there are regular singularities that are equilibria of the original system of differential equations. In addition, there are folded singularities that are not equilibria of the original system, but instead satisfy

$$f(V, c, n) = 0, \quad (14)$$

$$F(V, c, n) = 0, \quad (15)$$

$$\frac{\partial f}{\partial V} = 0. \quad (16)$$

From Eq. (16), the folded singularities occur on the fold curves L^- and L^+. For parameter values used in Fig. 2, the

system has a folded node, a folded singularity with two real negative eigenvalues, on L^+ (FN, in Fig. 2), and a folded focus (FF) (two complex eigenvalues with negative real parts) on L^- (not shown).

With the parameter values used in Fig. 2, there is a stable periodic orbit formed by solving Eqs. (11) and (12) on the upper and lower sheets, and following fast fibers upward or downward when the trajectory reaches a fold curve. This closed orbit, described in more detail in Ref. 18, is called a singular periodic orbit (SPO). In Fig. 2, this orbit moves through the folded node. Passage through the folded node is quite important, since away from the singular limit the slow manifold becomes twisted near the folded node, producing small oscillations in any trajectory entering this region. If the singular periodic orbit passes through the folded node, then when the singular parameter (C_m) is increased from 0 small oscillations will appear that are spikes of the pseudo-plateau burst.[18]

The singular periodic orbit and key curves are projected onto the (c, V)-plane in Fig. 3. Figure 3(a), which is the projection of Fig. 2, shows again that the singular periodic orbit passes through the folded node, so pseudo-plateau bursting is produced for $C_m > 0$ (Fig. 1(a)). However, when k_c is decreased from 0.16 $(ms)^{-1}$ (the value used in Figs. 1(a) and 3(a)) to 0.1 $(ms)^{-1}$, the singular periodic orbit does not pass through the folded node (Fig. 3(b)), so the model produces spiking instead of bursting when $C_m > 0$ (Fig. 1(c)). The orbit does not enter the folded node since when it reaches L^-

it moves to a point on $P(L^-)$ that is outside of the shaded region, called the singular funnel. Only points in the singular funnel move through the folded node.[28,30,31,33] The funnel is delimited by L^+ and the strong canard (SC, green curve), which is tangent to the strong eigenvector of the folded node (Fig. 3).

Decreasing f_c (the fraction of free calcium concentration in the cytosol) from 0.01 to 0.0025 moves the folded node and the strong canard rightward, so that the singular periodic orbit again enters the singular funnel (Fig. 3(c)). As a result, pseudo-plateau bursting is produced (Fig. 3(d)). Thus, reducing f_c compensates for the reduction in k_c, rescuing the bursting. This result would not have been predictable from the two-fast/one-slow analysis, which instead predicts a relaxation oscillation in the limit $f_c \rightarrow 0$ (cf. Fig. 1(d)).

V. THE RELATIONSHIP BETWEEN TWO-FAST/ONE-SLOW ANALYSIS AND ONE-FAST/TWO-SLOW ANALYSIS

A. The relationship between the V-nullcline and the z-curve

As shown in Fig. 4(a), the desingularized system (Eqs. (11) and (12)) has a single-branched V-nullcline (green curve) that satisfies $F(V, c, n) = 0$ and a three-branched c-nullcline (orange curves) L^-, L^+, and CN1. The fold curves L^-, L^+ satisfy $\frac{\partial f}{\partial V} = 0$. The curve CN1 satisfies

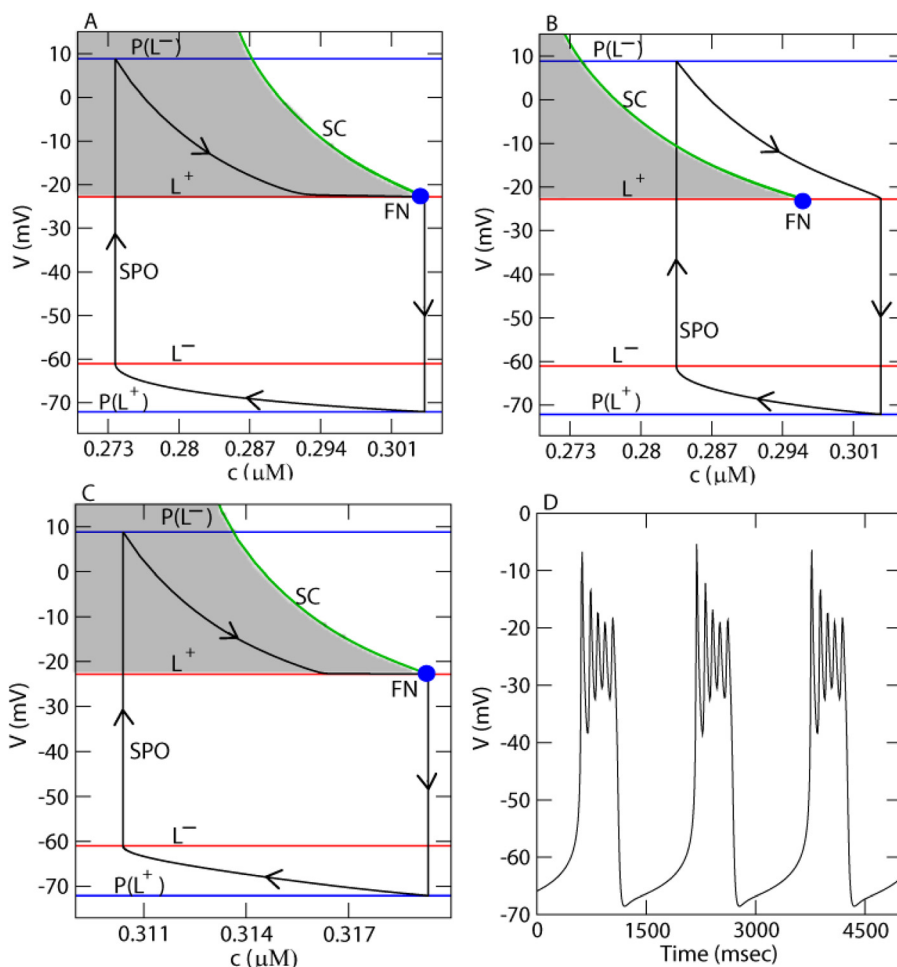
FIG. 3. The critical manifolds constructed with different parameter values are projected onto the (c, V)-plane. For all panels, $g_K = 4$ nS and $g_{BK} = 0.4$ nS. (a) $k_c = 0.16$ $(ms)^{-1}$ and $f_c = 0.01$. (b) $k_c = 0.1$ $(ms)^{-1}$ and $f_c = 0.01$. (c) $k_c = 0.1$ $(ms)^{-1}$ and $f_c = 0.0025$. The SPO (black curves with arrows) are superimposed. The singular periodic orbit is inside the singular funnel (shaded region) in panels (a) and (c), and outside of the singular funnel in panel (b). Lowering f_c to 0.0025 compensates for the decrease of k_c to 0.1 $(ms)^{-1}$, yielding pseudo-plateau bursting when $C_m = 10$ pF.
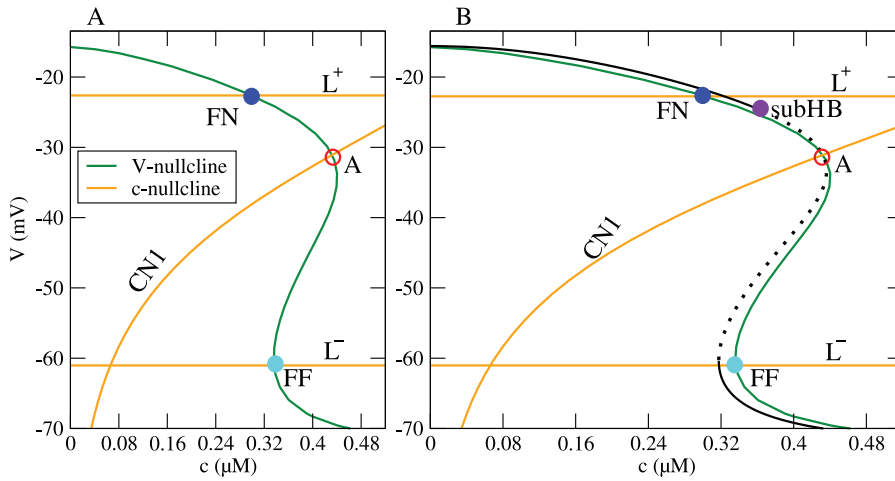
FIG. 4. The phase plane of the desingularized system with $g_K = 4\,\text{nS}$, $g_{BK} = 0.4\,\text{nS}$, $k_c = 0.16\,(\text{ms})^{-1}$ and $f_c = 0.01$. (a) The V-nullcline (green) intersects with the three-branched c-nullcline (orange) to form three singularities: a stable FN, a stable FF and an unstable ordinary singularity (A, unfilled circle). (b) The z-curve (black) with stable (solid) and unstable (dotted) branches of the fast subsystem in the two-fast/one-slow analysis, constructed with $C_m = 10\,\text{pF}$, is superimposed onto the (c, V)-phase plane of the desingularized system.

$\alpha I_{Ca} + k_c c = 0$, and is the c-nullcline of the full system, shown in Fig. 1(b). Folded singularities occur at the intersection of the V-nullcline with the fold curves L^- or L^+. In the case shown in Fig. 4(a), there are folded node and FF singularities. There is an unstable ordinary singularity (A, unfilled circle) that is located at an intersection of the V-nullcline with CN1. Since this singularity is an equilibrium of the full system, it is the same singularity as in Fig. 1(b), which occurs at the intersection of the c-nullcline and the z-curve. Figure 4(b) shows the superimposed z-curve (black curve) with stable (solid) and unstable (dotted) portions identified. The z-curve has almost the same shape as the V-nullcline, and the three curves (z-curve, V-nullcline, and CN1) intersect at the singular point A.

The z-curve satisfies $\frac{dV}{dt} = 0$ (in Eq. (1)) and $\frac{dn}{dt} = 0$ (in Eq. (2)), and the parameter $f_c = 0$ since c is treated as a parameter to construct this curve. The V-nullcline of the desingularized system is on S, so it satisfies $f(V, n, c) = 0$ and thus $\frac{dV}{dt} = 0$ (Eq. (1)). Because it is the V-nullcline of the desingularized system, $F(V, n, c) = 0$ (Eq. (11)). In the case of $f_c = 0$, Eq. (13) implies that either $\frac{(n_\infty(V) - n)}{\tau_n} = 0$ or $\frac{\partial f}{\partial n} = g_K(V - V_K) = 0$. Because the latter cannot occur (since $V > V_K$), $\frac{(n_\infty(V) - n)}{\tau_n} = 0$ on the V-nullcline when $f_c = 0$. From Eq. (2), $\frac{dn}{dt} = 0$ and therefore the V-nullcline of the desingularized system with $f_c = 0$ is identical to the z-curve from the two-fast/one-slow analysis.

Figure 5 shows the relationship between the two curves for three values of f_c. When f_c is decreased from 0.01 to 0.001, the upper portion of the V-nullcline and the folded node moves rightward. When $f_c = 0$, the V-nullcline lies on the z-curve. The folded node now lies on the z-curve (Fig. 5). Thus, slowing down the slower variable c moves the V-nullcline of the desingularized system toward the z-curve, but the folded node of the desingularized system and the subcritical Hopf bifurcation on the z-curve are still different.

B. The relationship between the folded singularities and the Hopf bifurcations

We now set f_c back to its default value and vary the speed of V through the parameter C_m. Changing C_m has no effect on the nullclines of the desingularized system (which

does not include C_m) or on the location of the z-curve (since $\frac{dV}{dt} = 0$ in Eq. (1)). However, the location of the subcritical Hopf bifurcation on the z-curve depends on C_m. When C_m is decreased, the subcritical Hopf bifurcation moves leftward on the z-curve, and by $C_m = 0.1\,\text{pF}$ another subcritical Hopf bifurcation (subHB2) has occurred on the lower branch of the z-curve (Fig. 6). Superimposing this curve onto the (c, V)-phase plane of the desingularized system shows that the subcritical Hopf bifurcation (subHB1) moves closer to the fold curve L^+ (Fig. 7).

Now, if f_c is again reduced the V-nullcline converges to the z-curve, so that the folded node and subcritical Hopf bifurcation are superimposed (Fig. 8(a)). In the double limit $f_c \to 0$, and $C_m \to 0$ the FN and subHB1 superimpose, as do the folded focus and subHB2 (Figs. 8(b) and 8(c)).

The convergence of folded singularities and subcritical Hopf bifurcations on the z-curve can be seen through an examination of the differential equations. We have seen that the V-nullcline converges to the z-curve as $f_c \to 0$. Thus, a folded singularity and a subcritical Hopf bifurcation lie on the same curve, and satisfy $\frac{dV}{dt} = 0$ and $\frac{dn}{dt} = 0$. The other
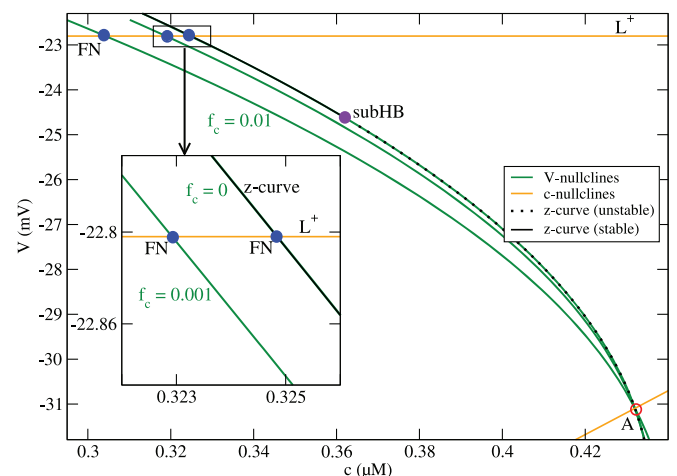

FIG. 5. The relationship between the V-nullcline and the z-curve with $g_K = 4\,\text{nS}$ and $k_c = 0.16\,(\text{ms})^{-1}$. Decreasing f_c causes the upper portion of the V-nullcline (green curve) and the folded node to move rightward. When $f_c = 0$, the V-nullcline and the z-curve (constructed with $C_m = 10\,\text{pF}$) superimpose, and the folded node lies on the z-curve.
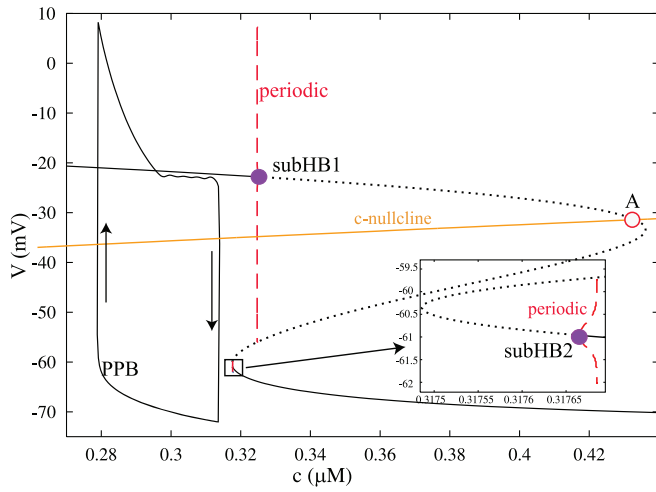
FIG. 6. Two-fast/one slow analysis for pseudo-plateau bursting with g_K = 4 nS and C_m = 0.1 pF. The reduction of C_m has moved the upper subcritical Hopf bifurcation (subHB1) and the associated unstable periodic branch leftward. This branch is now almost vertical. In addition, a new subcritical Hopf bifurcation (subHB2) is present on the lower branch of the z-curve. The PPB, produced with f_c = 0.01, does not follow the z-curve.

condition for a folded singularity is that it satisfies $\frac{\partial f}{\partial V} = 0$. Hence, what remains is to show that a subcritical Hopf bifurcation on the z-curve satisfies $\frac{\partial f}{\partial V} = 0$ in the case of $C_m \to 0$ pF. The z-curve is the curve of steady states of 1 and 2, and we can rewrite these as

$$\frac{dV}{dt} = \frac{1}{C_m} f(V, n) \quad (17)$$

and

$$\frac{dn}{dt} = g(V, n), \quad (18)$$

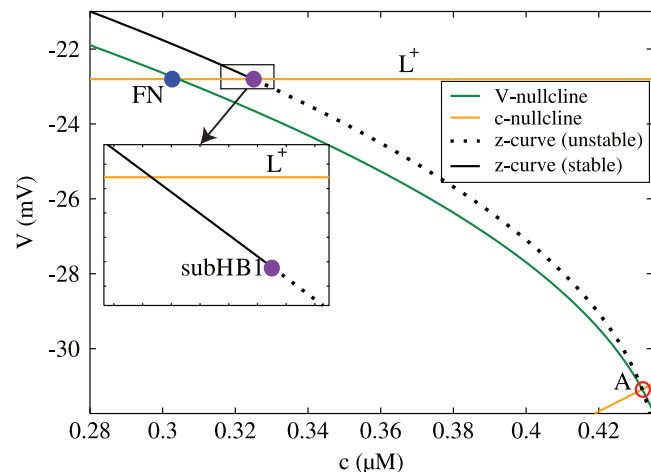where $g(V, n) = \frac{n_\infty(V) - n}{\tau_n}$. The Jacobian matrix of Eqs. (17) and (18) is

FIG. 7. The z-curve of the fast subsystem in the two-fast/one slow analysis constructed with g_K = 4 nS and C_m = 0.1 pF is superimposed into the (c, V)-phase plane of the desingularized system. The upper subcritical Hopf bifurcation is very close to the fold curve L^+.
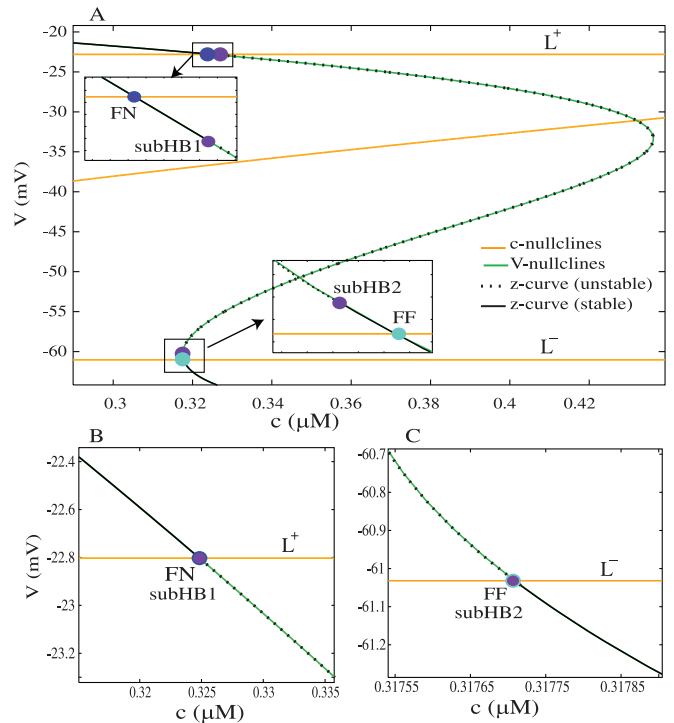

FIG. 8. The relationship between the folded singularities and the Hopf bifurcations in the double singular limit $f_c \to 0$ and $C_m \to 0$ pF. When $f_c \approx 0$, the V-nullcline (green curve) overlies the z-curve (black curve). (a) When C_m decreased to 0.1 pF, the upper subcritical Hopf bifurcation (subHB1) moves toward the folded node, and the lower subcritical Hopf bifurcation (subHB2) moves toward the folded focus. (b) When C_m = 0.0001 pF, the upper subcritical Hopf bifurcation has almost coalesced with the folded node. (c) When C_m = 0.0001 pF, the lower subcritical Hopf bifurcation has almost coalesced with the folded focus.

$$J = \begin{pmatrix} \frac{1}{C_m}\frac{\partial f}{\partial V} & \frac{1}{C_m}\frac{\partial f}{\partial n} \\ \frac{\partial g}{\partial V} & \frac{\partial g}{\partial n}, \end{pmatrix}, \quad (19)$$

and the trace of J is

$$\text{trace}(J) = \frac{1}{C_m}\frac{\partial f}{\partial V} + \frac{\partial g}{\partial n}. \quad (20)$$

Since $\text{trace}(J) = 0$ at a Hopf bifurcation, we have

$$\frac{\partial f}{\partial V} + C_m \frac{\partial g}{\partial n} = 0. \quad (21)$$

In the singular limit $C_m \to 0$ pF, the condition $\frac{\partial f}{\partial V} + C_m \frac{\partial g}{\partial n} = 0$ implies that $\frac{\partial f}{\partial V} = 0$. Hence, in the double limit $C_m \to 0$ pF and $f_c \to 0$, the folded singularities and the subcritical Hopf bifurcations satisfy $\frac{dV}{dt} = 0$, $\frac{dn}{dt} = 0$, and $\frac{\partial f}{\partial V} = 0$, and are identical points.

The z-curve constructed with two values of C_m is superimposed on the critical manifold in Fig. 9. Away from the singular limit, for example, when C_m = 10 pF, portions of the stable branches of the z-curve lie on the unstable middle sheet of the critical manifold (Fig. 9(a)). The subcritical Hopf and lower saddle-node bifurcations from which the stable branches of the z-curve emerge are also on the unstable middle sheet of the manifold. When C_m is decreased to
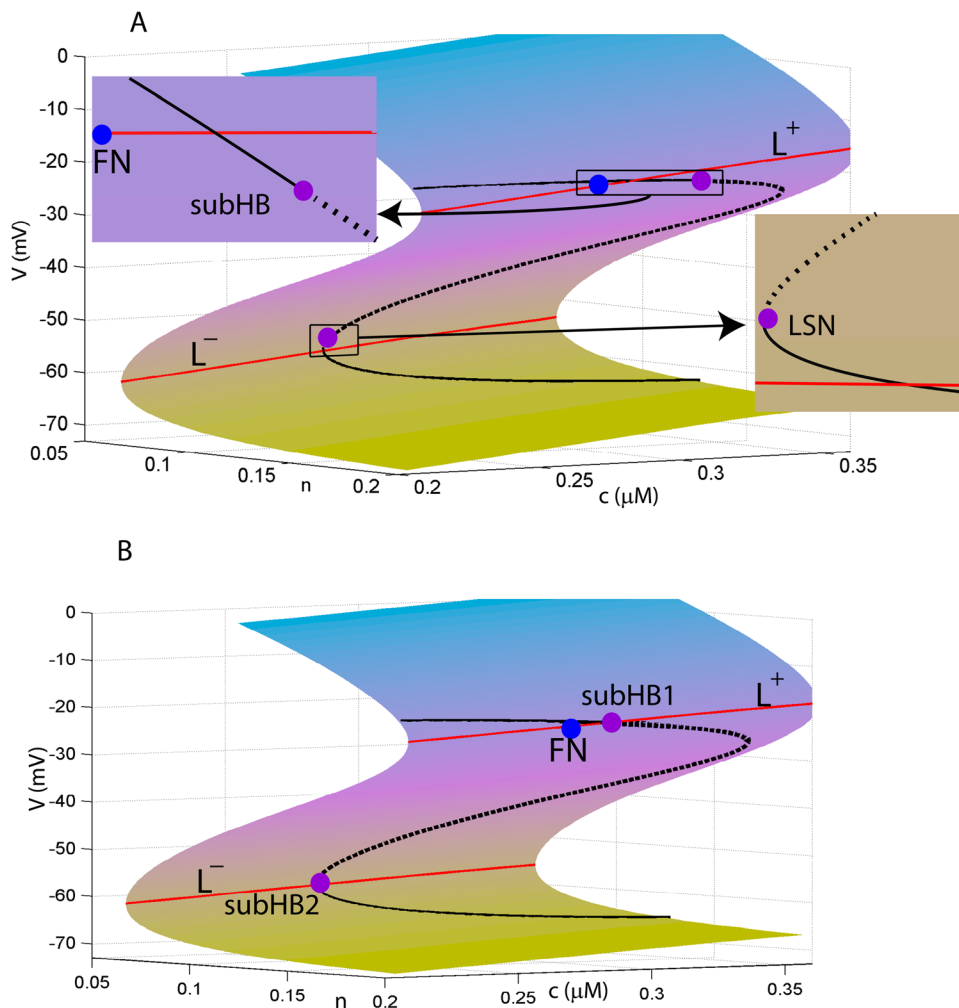
FIG. 9. The relationship between the z-curve (black curve) with stable (solid) and unstable (dotted) branches, and the critical manifold. The critical manifold is constructed with $f_c = 0.01$ and $C_m = 0\,\mathrm{pF}$ and is the same as in Fig. 2. (a) The z-curve is constructed with $C_m = 10\,\mathrm{pF}$ and superimposed. Portions of the stable branches lie on the repelling middle sheet of the critical manifold. The subcritical Hopf bifurcation and the lower saddle node (LSN) are on the repelling middle sheet. (b) The z-curve constructed with $C_m = 0.0001\,\mathrm{pF}$ now has its stable branches on the attracting sheets and unstable branch on the repelling sheet. The subcritical Hopf bifurcations lie on the fold curves.

0.0001 pF in Figure 9(b) stable branches of the z-curve move to the stable sheets of the critical manifold. Also, the subcritical Hopf bifurcations move to the fold curves.

VI. CONCLUSION

The lactotroph model that we analyzed is a three-dimensional system that produces fast oscillations clustered into periodic bursts. It is therefore natural to analyze the dynamics of the model by decomposing it into a fast subsystem and a slow subsystem. The standard fast/slow analysis considers two variables as fast, and one as slow.[9,16,19–21] This decomposition leads to several key structures such as the slow manifold or "z-curve" and the Hopf bifurcation that gives rise to a branch of periodic spiking solutions. An alternate decomposition, in which one variable is considered fast and two variables are considered slow, has recently been used to analyze fast bursting in pituitary cells.[17,18] This decomposition leads to a different set of key structures: the critical manifold, nullclines of the desingularized system, and folded node singularities. In this article, we have shown the relationship between the key structures of both forms of fast/slow analysis.

The z-curve is the set of stationary solutions of the planar fast subsystem in the two-fast/one-slow analysis. We have shown that this curve lies on the critical manifold obtained in the one-fast/two-slow analysis (Fig. 9). The unstable portion of the z-curve lies in the repelling middle sheet of the critical manifold, as do portions of the stable branches (Fig. 9(a)). When the voltage variable V is made to change very rapidly ($C_m \to 0$) the stable portions of the z-curve move solely to stable sheets of the critical manifold (Fig. 9(b)).

The z-curve also lies close to the V-nullcline of the desingularized system. Decreasing the speed of the slower variable c moves the V-nullcline to the z-curve. When c is extremely slow ($f_c \to 0$), the V-nullcline is superimposed onto the z-curve (Fig. 5). The folded node also lies on the z-curve in this limit, but it is away from the subcritical Hopf bifurcation. When V is very fast the subcritical Hopf bifurcation moves upward to the folded node and becomes singular. In the singular limits ($f_c \to 0$ and $C_m \to 0$) the folded node and the subcritical Hopf bifurcation are identical (Fig. 8).

Which structures are organizing the dynamics, the z-curve and Hopf bifurcation, or the V-nullcline and folded node? This depends on the timescale relationship between the variables. As we see in Fig. 10(a), when V is not too fast and c is not too slow the burst trajectory (brown) follows neither the z-curve of the two-fast/one-slow decomposition nor the V-nullcline of the one-fast/two-slow decomposition. When c is very slow, the trajectory follows the z-curve
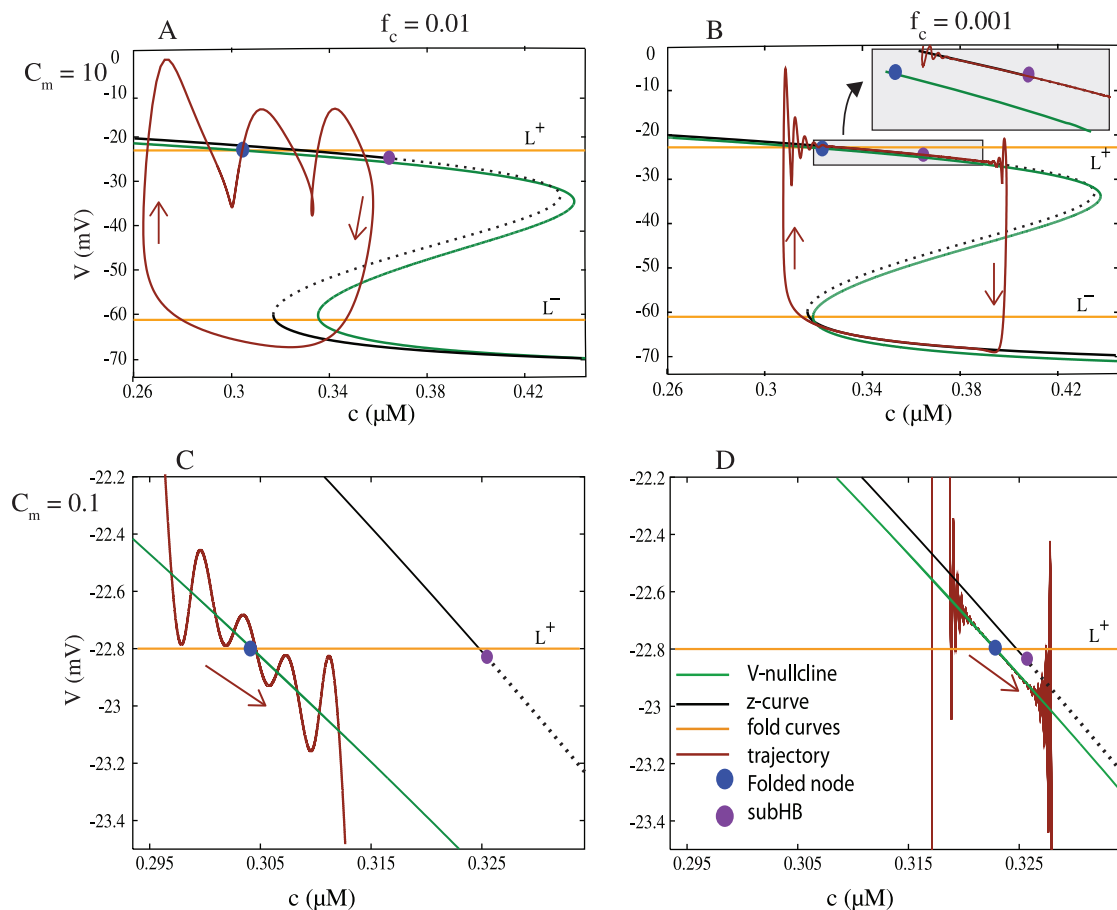
FIG. 10. The relationship of the burst trajectory (brown) with the z-curve (black) and the V-nullcline of the desingularized system (green). (a) With C_m = 10 pF and f_c = 0.01, the burst trajectory follows neither the z-curve nor the V-nullcline. (b) With C_m = 10 pF and f_c = 0.001, the burst trajectory moves along the upper and lower branches of the z-curve. The trajectory passes through the subcritical Hopf bifurcation (magenta circle). (c) With C_m = 0.1 pF and f_c = 0.01, the burst trajectory oscillates around the V-nullcline, and passes very close to the folded node (blue circle). (d) With C_m = 0.1 pF and f_c = 0.001, the burst trajectory oscillates around the V-nullcline and passes through the folded node. The z-curve and subcritical Hopf bifurcation are located nearby.

closely (Fig. 10(b)). It follows the bottom branch during the silent phase and the top branch during the active phase, jumping down after a slow passage through the subcritical Hopf bifurcation.[34] On the other hand, when V is very fast, the trajectory oscillates around the V-nullcline of the desingularized system and passes very close to the folded node (Fig. 10(c)). The amplitude of the oscillations first decreases and then increases, as typical for oscillations associated with a folded node singularity.[35] When V is very fast and c is very slow the trajectory again moves along the V-nullcline and through the folded node (Fig. 10(d)). In this case, the z-curve and subcritical Hopf bifurcation are located nearby. Thus, either technique may provide a good description of the dynamics, depending on how close the system is to the appropriate singular limit.

The two analysis techniques lead to predictions that can be tested experimentally using the Dynamic Clamp technique.[36] For example, the two-fast/one-slow analysis technique tells us that if the hyperpolarizing delayed rectifier K⁺ conductance g_K is reduced sufficiently, then the bursting should be replaced by a depolarized steady state. The one-fast/two-slow analysis tells us even more: small decreases in g_K should increase the duration of a burst by adding more spikes. Likewise, the one-fast/two-slow analysis tells us that increasing the BK conductance g_{BK} should convert many

spiking cells to a bursting state, and should increase the burst duration of those cells that are already bursting. This prediction was tested experimentally and validated.[10] In summary, the different fast/slow decompositions tell us useful information about a model cell's dynamics, and with the dynamic clamp technique, often in combination with pharmacological agents, these model predictions can be and have been tested.

ACKNOWLEDGMENTS

APPENDIX: THE LACTOTROPH MODEL

The lactotroph model is described by Eqs. (1)–(7) given earlier, along with the additional equations and parameters given here (Table I). The steady state activation functions are given by:

$$m_\infty(V) = \left(1 + \exp\left(\frac{v_m - V}{s_m}\right)\right)^{-1}, \qquad (A1)$$

TABLE I. Parameter values for the lactotroph model.

Parameter	Value	Description
C_m	5 pF	Membrane capacitance of the cell
g_{Ca}	2 nS	Maximum conductance of Ca^{2+} channels
V_{Ca}	50 mV	Reversal potential for Ca^{2+}
v_m	−20 mV	Voltage value at midpoint of m_∞
s_m	12 mV	Slope parameter of m_∞
g_K	4 nS	Maximum conductance of K^+ channels
V_K	−75 mV	Reversal potential for K^+
v_n	−5 mV	Voltage value at midpoint of n_∞
s_n	10 mV	Slope parameter of n_∞
τ_n	43 ms	Time constant of n
$g_{K(Ca)}$	1.7 nS	Maximum conductance of K(Ca) channels
K_d	0.5 μM	c at midpoint of s_∞
g_{BK}	0.4 nS	Maximum conductance of BK-type K^+ channels
v_b	−20 mV	Voltage value at midpoint of f_∞
s_b	5.6 mV	Slope parameter of f_∞
f_c	0.01	Fraction of free Ca^{2+} ions in cytoplasm
α	0.0015 μM pA^{-1}	Conversion from charge to concentration
k_c	0.16 ms^{-1}	Rate of Ca^{2+} extrusion

$$n_\infty(V) = \left(1 + \exp\left(\frac{v_n - V}{s_n}\right)\right)^{-1}, \qquad \text{(A2)}$$

$$s_\infty(c) = \frac{c^2}{c^2 + K_d^2}, \qquad \text{(A3)}$$

$$b_\infty(V) = \left(1 + \exp\left(\frac{v_b - V}{s_b}\right)\right)^{-1}. \qquad \text{(A4)}$$

The variables V, n, and c vary on different time scales. The time constant for n is $\tau_n = 43$ ms. The time constant of V is given by $\tau_V = C_m/g_{Total}$, where $g_{Total} = g_K n + g_{BK} b_\infty(V) + g_{Ca} m_\infty(V) + g_{K(Ca)} s_\infty(c)$. During a bursting oscillation, V ranges from −70 mV to 2 mV, and the minimum of g_{Total} is 0.483 nS and the maximum is 3 nS. Hence, $\frac{C_m}{max g_{Total}} \leq \tau_V \leq \frac{C_m}{min g_{Total}}$, or 1.7 ms $\leq \tau_V \leq$ 10.4 ms, for $C_m = 5$ pF, a typical capacitance value for lactotrophs. The time constant for c is $\frac{1}{f_c k_c} = \frac{1}{(0.01)(0.16)}$ ms $= 625$ ms. Thus, V is fast, n is intermediate and c is slow.

[1] W. T. Frazier, E. R. Kandel, I. Kupfermann, R. Waziri, and R. E. Coggeshall, "Morphological and functional properties of identified neurons in the abdominal ganglion of *Aplysia californica*," J. Neurophysiol. **30**, 1288–1351 (1967).

[2] R. J. Butera, J. Rinzel, and J. C. Smith, "Models of respiratory rhythm generation in the pre-Bötzinger complex. I. Bursting pacemaker neurons," J. Neurophysiol. **82**, 382–397 (1999).

[3] C. A. Del Negro, C.-F. Hsiao, and S. H. Chandler, "Outward currents influencing bursting dynamics in guinea pig trigeminal motoneurons," J. Neurophysiol. **81**, 1478–1485 (1999).

[4] V. F. Safiulina, P. Zacchi, M. Taglialatela, Y. Yaari, and E. Cherubini, "Low expression of Kv7/M channels facilitates intrinsic and network bursting in the developing rat hippocampus," J. Physiol. **586**, 5437–5453 (2008).

[5] D. Lyons, E. Horjales-Araujo, and C. Broberger, "Synchronized network oscillations in rat tuberoinfundibular dopamine neurons: Switch to tonic discharge by thyrotropin-releasing hormone," Neuron **65**, 217–229 (2010).

[6] Y. A. Kuryshev, G. V. Childs, and A. K. Ritchie, "Corticotropin-releasing hormone stimulates Ca^{2+} entry through L- and P-type Ca^{2+} channels in rat corticotropes," Endocrinology **137**, 2269–2277 (1996).

[7] F. Van Goor, D. Zivadinovic, A. J. Martinez-Fuentes, and S. S. Stojilkovic, "Dependence of pituitary hormone secretion on the pattern of spontaneous voltage-gated calcium influx. Cell type-specific action potential secretion coupling," J. Biol. Chem. **276**, 33840–33846 (2001).

[8] S. S. Stojilkovic, H. Zemkova, and F. Van Goor, "Biophysical basis of pituitary cell type-specific Ca^{2+} signaling-secretion coupling," Trends Endocrinol. Metab. **16**, 152–159 (2005).

[9] K. Tsaneva-Atanasova, A. Sherman, F. Van Goor, and S. S. Stojilkovic, "Mechanism of spontaneous and receptor-controlled electrical activity in pituitary somatotrophs: Experiments and theory," J. Neurophysiol. **98**, 131–144 (2007).

[10] J. Tabak, M. Tomaiuolo, A. Gonzalez-Iglesias, L. Milescu, and R. Bertram, "Fast-activating voltage-and calcium-dependent potassium BK conductance promotes bursting in pituitary cells: A dynamic clamp study," J. Neurosci. **31**, 16855–16863 (2011).

[11] J. E. Lisman, "Bursts as a unit of neural information: Making unreliable synapses reliable," Trends Neurosci. **20**, 38–43 (1997).

[12] R. Plant and M. Kim, "On the mechanism underlying bursting in the Aplysia abdominal ganglion R15 cell," Math. Biosci. **26**, 357–375 (1975).

[13] T. Chay and J. Keizer, "Minimal model for membrane oscillations in the pancreatic β-cell," Biophys. J. **42**, 181–190 (1983).

[14] A. P. LeBeau, A. B. Robson, A. E. McKinnon, and J. Sneyd, "Analysis of a reduced model of corticotroph action potentials," J. Theor. Biol. **192**, 319–339 (1998).

[15] R. Bertram and A. Sherman, "A calcium-based phantom bursting model for pancreatic islets," Bull. Math. Biol. **66**, 1313–1344 (2004).

[16] J. Tabak, N. Toporikova, M. E. Freeman, and R. Bertram, "Low dose of dopamine may stimulate prolactin secretion by increasing fast potassium currents," J. Comput. Neurosci. **22**, 211–222 (2007).

[17] T. Vo, R. Bertram, J. Tabak, and M. Wechselberger, "Mixed mode oscillations as a mechanism for pseudo-plateau bursting," J. Comput. Neurosci. **28**, 443–458 (2010).

[18] W. Teka, J. Tabak, T. Vo, M. Wechselberger, and R. Bertram, "The dynamics underlying pseudo-plateau bursting in a pituitary cell model," J. Math. Neurosci. **1**, 12 (2011).

[19] J. Rinzel, "A formal classification of bursting mechanisms in excitable systems," in *Mathematical Topics in Population Biology, Morphogenesis, and Neurosciences, Lecture Notes in Biomathematics*, edited by E. Teramoto and M. Yamaguti (Springer, Berlin, 1987), pp. 267–281.

[20] R. Bertram, M. J. Butte, T. Kiemel, and A. Sherman, "Topological and phenomenological classification of bursting oscillations," Bull. Math. Biol. **57**, 413–439 (1995).

[21] J. Rinzel and G. B. Ermentrout, "Analysis of neural excitability and oscillations," in *Methods in Neuronal Modeling: From Synapses to Networks*, 2nd ed., edited by C. Koch and I. Segev (MIT, Cambridge, MA, 2003), pp. 251–292.

[22] H. M. Osinga and K. Tsaneva-Atanasova, "Dynamics of plateau bursting depending on the location of its equilibrium," J. Neuroendocrinol. **22**, 1301–1314 (2010).

[23] J. Nowacki, S. Mazlan, H. M. Osinga, and K. Tsaneva-Atanasova, "The role of large-conductance calcium-activated K^+ (BK) channels in shaping bursting oscillations of a somatotroph cell model," Physica D **239**, 485–493 (2010).

[24] W. Teka, K. Tsaneva-Atanasova, R. Bertram, and J. Tabak, "From plateau to pseudo-plateau bursting: Making the transition," Bull. Math. Biol. **73**, 1292–1311 (2011).

[25] R. Bertram and A. Sherman, "Negative calcium feedback: The road from Chay-Keizer," in *The Genesis of Rhythm in the Nervous System*, edited by S. Coombes and P. Bressloff (World Scientific, New Jersey, 2005), pp. 19–48.

[26] J. V. Stern, H. M. Osinga, A. LeBeau, and A. Sherman, "Resetting behavior in a model of bursting in secretory pituitary cells: Distinguishing plateaus from pseudo-plateaus," Bull. Math. Biol. **70**, 68–88 (2008).

[27] M. Brøns, M. Krupa, and M. Wechselberger, "Mixed mode oscillations due to the generalized canard phenomenon," Fields Inst. Commun. **49**, 39–63 (2006).

[28] P. Szmolyan and M. Wechselberger, "Canards in $\mathbb{R}^3$," J. Differ. Equations. **177**, 419–453 (2001).

[29] H. G. Rotstein, M. Wechselberger, and N. Kopell, "Canard induced mixed-mode oscillations in a medial entorhinal cortex layer II stellate cell model," SIAM J. Appl. Dyn. Syst. **7**, 1582–1611 (2008).

[30] M. Wechselberger, "Existence and bifurcation of canards in $\mathbb{R}^3$ in the case of a folded node," SIAM J. Appl. Dyn. Syst. **4**, 101–139 (2005).

[31]M. Desroches, J. Guckenheimer, B. Krauskopf, C. Kuehn, H. Osinga, and M. Wechselberger, "Mixed-mode oscillatons with multiple time-scales," SIAM Rev. **54**, 211–288 (2012).

[32]B. Ermentrout, *Simulating, Analyzing, and Animating Dynamical Systems: A guide to XPPAUT for Researchers and Students* (SIAM, Philadelphia, 2002).

[33]M. Wechselberger, "A propos de canards (apropos canards)," Trans. Am. Math. Soc. **364**, 3289–3309 (2012).

[34]S. M. Baer, T. Erneux, and J. Rinzel, "The slow passage through a Hopf bifurcation: Delay, memory effects, and resonance," SIAM J. Appl. Math. **49**, 55–71 (1989).

[35]J. Guckenheimer, "Singular Hopf bifurcation in systems with two slow variables," SIAM J. Appl. Dyn. Syst. **7**, 1355–1377 (2008).

[36]L. Milescu, T. Yamanishi, K. Ptak, M. Mogri, and J. Smith, "Real-time kinetic modeling of voltage-gated ion channels using dynamic clamp," Biophys. J. **95**, 66–87 (2008).